Stability in Active Mass Damping Control of a Flexible Robot

Ryan W. Krauss and Wayne J. Book
George W. Woodruff School of Mechanical Engineering
Georgia Institute of Technology
Atlanta, GA 30332
gtg708j@mail.gatech.edu, wayne.book@me.gatech.edu

ABSTRACT

Active mass damping has been shown to be an effective method for reducing vibrations in flexible robots by previous researchers working on an experimental test bed at Georgia Tech. Acceleration feedback can cause instability in this test bed. System identification and root locus analysis were used to determine the causes of this instability. Several potential modifications to the system were simulated including 1) replacing accelerometers with position sensors, 2) removing second order dynamics from the actuator, and 3) adding an additional accelerometer to use modal feedback.

TABLE OF CONTENTS

1. INTRODUCTION

Active mass damping has been shown to be an effective method for reducing vibrations in flexible robots by previous researchers working on an experimental test bed at Georgia Tech [1], [2], [3], [4], [5]. The experimental test bed is shown in Figure 1. The experimental test bed consists of a rigid micro-manipulator mounted on the free end of a cantilevered beam. The micro-manipulator is referred to by the acronym SAMII which stands for Small Articulated Manipulator II. The cantilevered beam serves as a flexible base for SAMII. This base represents a macro-manipulator with its joints locked. The cantilevered beam that serves as SAMII's flexible base is approximately 5 meters long. SAMII has six joints all of which are actuated by hydraulic rotary motors and Moog servo-valves.

0-7803-8155-6/04/$17.00/©2004 IEEE
IEEEAC paper #1188

Base acceleration feedback can cause this system to become unstable. There are several suspected causes of this instability. The first is that in order to generate interaction forces that damp base vibrations, the input voltage to the hydraulic actuator should ideally be proportional to the base position. The existing test bed uses an accelerometer attached to the base instead. For sinusoidal base vibrations of frequency ω, this means that the input signal differs from the ideal case by a factor of $-\omega^2$. This means that the effective gain at the second natural frequency of the base is significantly higher than the gain at the first natural frequency.

A second suspected cause of instability is a 90° difference between the expected and actual phase lag of the actuator over a frequency band near the second natural frequency of the base. This drop off in phase appears to come from a second-order pole and a second-order zero that are in close proximity in the complex plane, as can be seen in an experimental Bode plot of the hydraulic actuator (Figure 2). This deviation of the system from the pure integrator model can be explained by interaction between the actuator and the flexible base.

A third potential source of instability is the inability to separate force and torque interactions in the current experimental configuration. The first mode of the base is primarily excited by the interaction force while the second mode is more susceptible to the interaction torque. A potential solution to this problem would be to use a 6 DOF micro-manipulator capable of generating desired interaction forces and torques separately.

2. SUSPECTED CAUSES OF INSTABILITY

In attempting to recreate the mass damping controller in [4], the experimental system was found to deviate from the model used to design the controller in two key ways. The first is that interaction with the flexible base keeps the hydraulic actuator from responding as a pure integrator. The second is that the system uses accelerometers rather than position sensors to feedback base motion.

Actuator Phase Error

Figure 2 compares the pure integrator model to the experimental Bode response of the system. Near the second natural

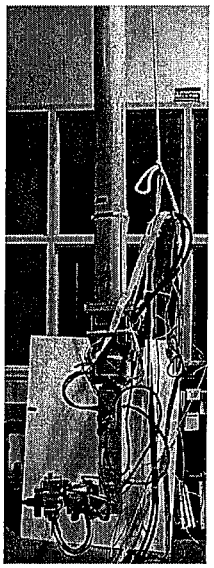

Figure 1. SAMII: Small Articulated Manipulator II. SAMII is a rigid micro-manipulator attached to flexible base.

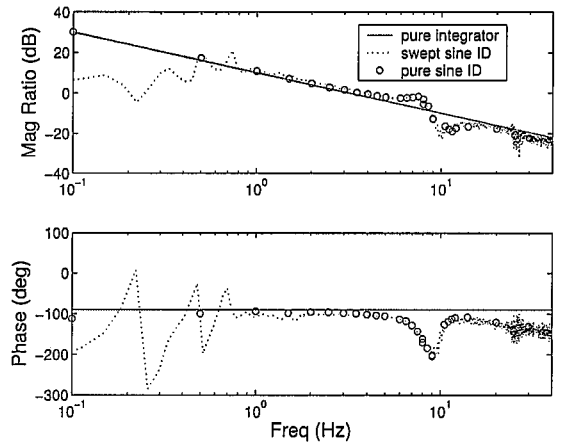

Figure 2. Comparison of bode plots from a pure integrator model and experimental data for the hydraulic actuator.

frequency of the flexible base (10Hz), the phase of the model is off by 90°. When trying to add damping to the system, a phase error of 90° seems significant. Instead of adding damping to the system, this phase error could lead to driving the system at resonance and may be the cause of instability in the system.

The Need for Position Sensors

A brief explanation of the authors' interpretation of the controller used in [4] will highlight the need for position sensors. Using accelerometers instead of position sensors causes the effective gain on the second mode to be ω_2^2/ω_1^2 times greater than the effective gain on the first mode. This may contribute to instability.

In order to use the micro-manipulator to add damping to the flexible base, the mass damping controller needs to cause an interaction force $\bar{F}_{md}$ proportional to $-\dot{\bar{x}}$ or

$$\bar{F}_{md} = -\mathbf{K_a}\dot{\bar{\mathbf{x}}} \tag{1}$$

where $\mathbf{K_a}$ is a diagonal gain matrix and $\dot{\bar{x}}$ is the velocity of the end of the cantilevered beam (the point where the interaction force is applied to the base). Equation 1 represents the desired interaction force for the mass damping controller.

The actual interaction force caused by motion of the micro-manipulator will be

$$\bar{F}_{md} \approx \mathbf{B_f}\ddot{\bar{\theta}} \tag{2}$$

where $\mathbf{B_f}$ is a configuration dependent matrix relating inertial interaction forces to motions of the micro-manipulator joints. (This assumes that Coriolis and centrifugal terms can be neglected.)

Each joint of the micro-manipulator is controlled by a servovalve. If the actuator can be modeled as an integrator, the transfer function between angular position and input voltage for each joint is

$$\frac{\theta_i}{v_i} = \frac{K_{1i}}{s} \tag{3}$$

and

$$\ddot{\bar{\theta}} \approx s\mathbf{K_1}\bar{\mathbf{v}} \tag{4}$$

where $\mathbf{K_1}$ is a diagonal matrix of constant gains made up of the numerators of the transfer functions represented in equation 3. (Note that in this derivation, initial conditions are being ignored so that time domain variables and their transforms are used interchangeably).

Setting the desired and actual interaction forces of equations 1 and 2 equal to each other, substituting for $\ddot{\bar{\theta}}$ from equation 4, and solving for $\bar{v}$ gives

$$\bar{v} = -\mathbf{K_1}^{-1}\mathbf{B_f}^{-1}\mathbf{K_a}\bar{\mathbf{x}}. \tag{5}$$

Using an accelerometer rather than a position sensor, the mass damping voltage would be

$$\bar{v} = -\frac{1}{s^2}\mathbf{K_1}^{-1}\mathbf{B_f}^{-1}\mathbf{K_a}\ddot{\bar{\mathbf{x}}}. \tag{6}$$

The double integration specified by equation 6 poses a problem if the acceleration has even a small d.c. offset. This signal cannot be effectively high pass filtered without significant impact on the phase because the first natural frequency of the base is 1.75Hz. The phase is particularly important because the controller is trying to add damping to the system.

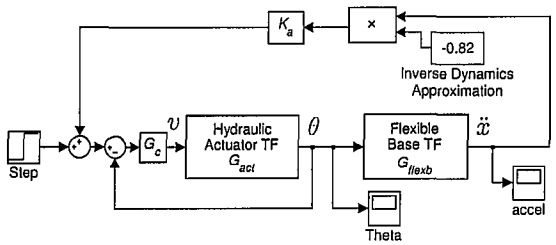

Figure 3. Block diagram of the mass damping control system. (This system is unstable.)

In order to avoid double integrating $\ddot{x}$, it was assumed that $\ddot{x}$ was composed primarily of a single sine wave, namely the first mode of vibration of the base. This simplification seems to line up with experimental observations. This simplification allows double integration to be replaced by division by $-\omega_1^2$. The risk associated with this simplification is that if the second mode is present, the effective gain on that mode will be ω_2^2/ω_1^2 times higher than the effective gain on the first mode.

Substituting $-1/\omega_1^2$ for $1/s^2$ in equation 6 gives the initial form used for mass damping control based on acceleration feedback

$$\bar{v} = \frac{1}{\omega_1^2}\mathbf{K_1}^{-1}\mathbf{B_f}^{-1}\mathbf{K_a}\ddot{\mathbf{x}} \tag{7}$$

3. Bode System Identification

Figure 3 shows a block diagram of a simplified model of the system. Figures 4 and 5 show the results of curve fitting models to the experimental Bode data.

The form of the model used to fit the data in Figure 4 is

$$G_{act} = \frac{\theta}{v} = \frac{K_1{\omega_d}^2\left(s^2 + 2\zeta_2\omega_2 s + {\omega_2}^2\right)\tau}{s{\omega_2}^2\left(s^2 + 2\zeta_d\omega_d s + {\omega_d}^2\right)(s+\tau)}. \tag{8}$$

This form could be derived based on linearizing the equations of motion for a hydraulic actuator mounted between a mass and a flexible base in a manner similar that in [6, pp.176-181].

The form of the model used to fit the data in Figure 5 is

$$G_{flexb} = \frac{\ddot{x}}{\theta} = \frac{s^4 B_1\phi_1(L)}{s^2 + 2\zeta_1\omega_1 s + w_1^2} + \frac{s^4 B_2\phi_2(L)}{s^2 + 2\zeta_2\omega_2 s + \omega_2^2}. \tag{9}$$

This form is based on assuming the flexible base has two modes whose equations of motion can be written as

$$\ddot{q}_1 + 2\zeta_1\omega_1\dot{q}_1 + \omega_1^2 q_1 = B_1\ddot{\theta} \tag{10}$$

$$\ddot{q}_2 + 2\zeta_2\omega_2\dot{q}_2 + \omega_2^2 q_2 = B_2\ddot{\theta} \tag{11}$$

where q_1 and q_2 are the amplitudes of the first two modes of the beam. The displacement of the end of the beam will be

$$x = \phi_1(L)q_1 + \phi_2(L)q_2 \tag{12}$$

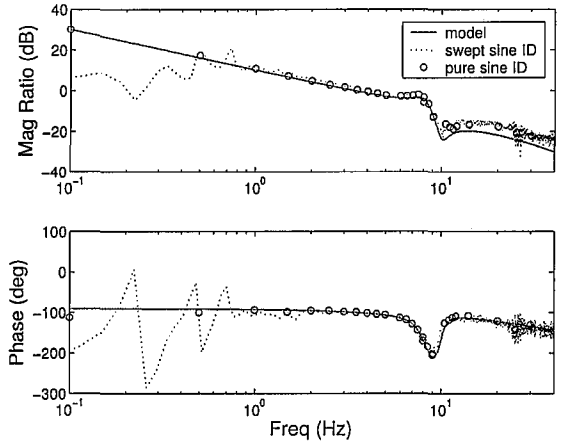

Figure 4. Results of fitting a model of the form given in equation 4 to experimental data for the hydraulic actuator.

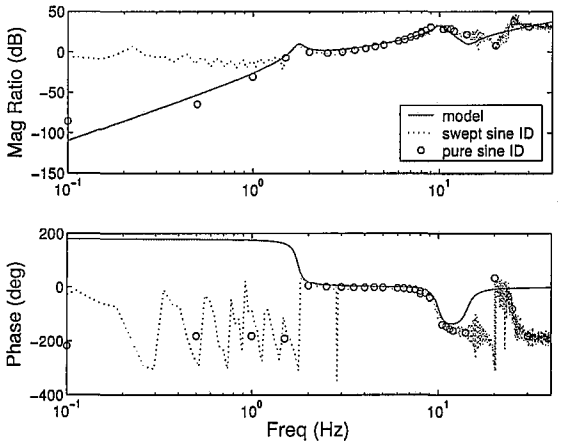

Figure 5. Results of fitting a model of the form given in equation 9 to experimental data for the flexible base.

where ϕ_1 and ϕ_2 are the mode shapes (L is the length of the beam).

The transfer function between tip displacement and angular acceleration is

$$\frac{x}{\ddot{\theta}} = \frac{B_1\phi_1(L)}{s^2 + 2\zeta_1\omega_1 s + w_1^2} + \frac{B_2\phi_2(L)}{s^2 + 2\zeta_2\omega_2 s + \omega_2^2}. \tag{13}$$

Measuring base acceleration rather than base position and θ rather then $\ddot{\theta}$ changes the transfer function from that given by equation 13 to that given by equation 9.

In order to correctly fit the data of Figure 5, B_1 of equation 9 must be negative and B_2 must be positive. This difference in sign between these two coefficients is a significant cause of instability as will be seen in Section 4.

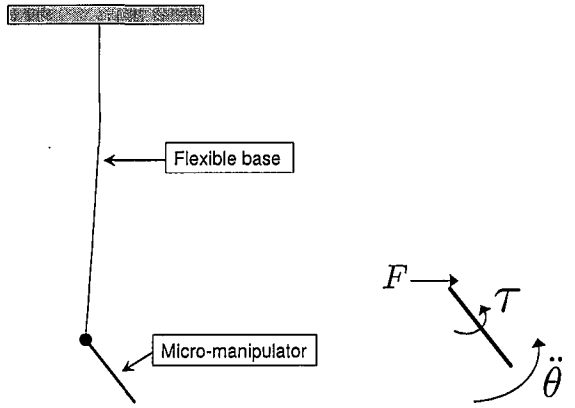

Figure 6. Schematic of the micro-manipulator at the end of the flexible base (left) and a free body diagram of the micro-manipulator (right).

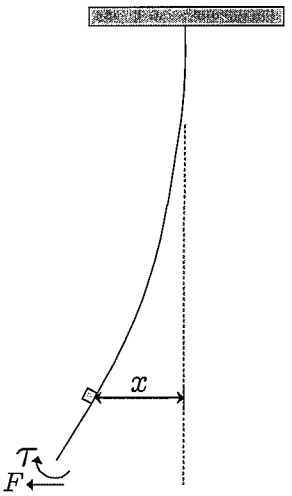

Figure 7. Expected mode shape for the first mode of the cantilevered beam.

The reason B_1 and B_2 are of opposite sign is that the second mode shape of the cantilevered beam differs from what would be expected without a mass attached to the end of the beam. Figure 6 shows a schematic of the system and a free body diagram of the micro-manipulator including the interaction force and torque required to cause a counterclockwise $\ddot{\theta}$. Figure 7 shows the expected first mode response to the equal and opposite interaction force and torque. Figure 8 shows the actual deflection shape experimentally observed while exciting the system near the second natural frequency. Note that the accelerometer (the small square) moves in opposite directions in Figures 7 and 8. The accelerometer moving in opposite directions with respect to $\ddot{\theta}$ at the two natural frequencies explains why B_1 and B_2 are of opposite sign.

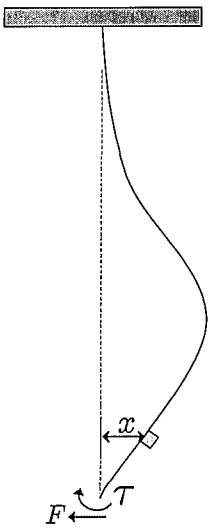

Figure 8. Actual deflection shape near the second natural frequency of the cantilevered beam. The motion of the accelerometer in this case is the opposite of that seen in Figure 7.

4. Root Locus Analysis

In order to use root locus to analyze the system in Figure 3, the transfer function between $\ddot{x}$ and v must be found. The motion control and vibration suppression are designed independently. This allows the feedback loop containing G_c and the hydraulic actuator transfer function (θ/v) to be replaced by the closed loop transfer function

$$G_{\theta cl} = \frac{\theta_{cl}}{v} = \frac{G_c G_{act}}{1 + G_c G_{act}} \tag{14}$$

where G_{act} is given by equation 8.

The transfer function for the flexible base is given by equation 9. The overall transfer function between base acceleration $\ddot{x}$ and servo-valve voltage is given by

$$\frac{\ddot{x}}{v} = \frac{G_{\theta cl} G_{flexb}}{1 + 0.82 K_a G_{\theta cl} G_{flexb}}. \tag{15}$$

The effects of varying the constant gain K_a can now be investigated using root locus.

The Effect of B_1 Being Negative

Figure 9 shows a root locus for the mass damping control system without any modifications. As K_a is increased, the system goes unstable before there is any significant improvement in the vibration response.

Figure 10 zooms in on the portion of the locus near the origin. Please note that the pole in Figure 9 at approximately -170

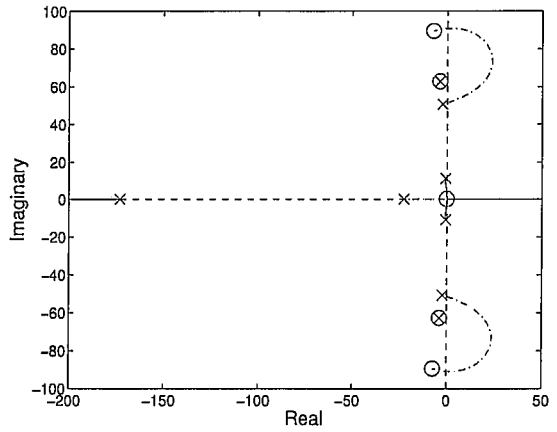

Figure 9. Root locus of the mass damping system without any modifications.

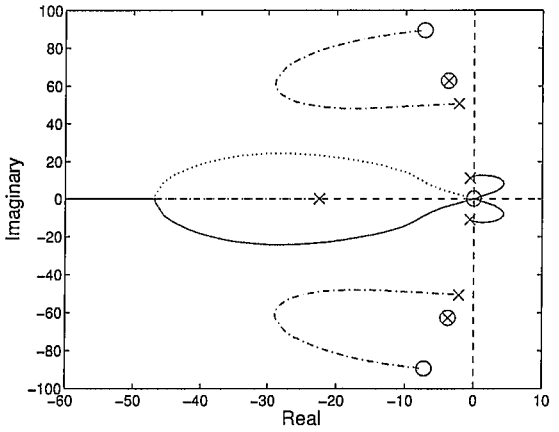

Figure 11. Root locus of the mass damping system without any modifications. The gain K_a is negative.

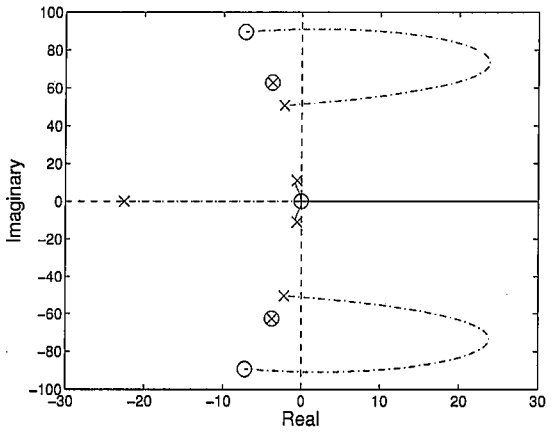

Figure 10. Root locus of the mass damping system without any modifications. (Zooming in on Figure 9.)

on the real axis is at this same location in all of the loci in this paper. All of the subsequent loci will zoom in closer to the origin so that this pole is not visible.

Since B_1 is negative, all of the numerator coefficients in the transfer function $\ddot{x}/v$ are negative, resulting in a root locus with an angle criterion of 0° rather than 180°. Since B_1 is negative, it seemed necessary to investigate the system with the gain K_a negative as well. The root locus for the unmodified system with K_a negative is shown in Figure 11. Again, the system goes unstable before there is a significant improvement in the vibration response.

The significance of B_1 being negative can be seen from equations 10 and 11. If $\ddot{\theta}$ is specified so that $B_1\ddot{\theta}$ is adding damping to equation 10, then $B_2\ddot{\theta}$ will be subtracting damping from equation 11. Since both modes are lightly damped, very little damping can be subtracted before the overall damping is negative and the mode is unstable. This explains why in the root locus shown in Figure 10 the poles for the first mode are moving to the left (increasing damping) while the poles for the second mode are moving to the right (decreasing damping) and become unstable. With the gain K_a negative in Figure 11, the poles from the second mode move toward increasing damping while the ones from the first mode move toward decreasing damping and become unstable.

Simulating Changes to the System

In order to improve system performance and overcome the instabilities, root locus analysis was performed on two potential system modifications: 1) replacing the actuator model with a pure integrator and 2) replacing the accelerometers with position sensors.

Figures 12 and 13 show the changes to the root locus resulting from eliminating the phase difference between the pure integrator model and the experimentally determined actuator transfer function near the second natural frequency of the base. This root locus simulates the system response if the actuator was actually a pure integrator. This eliminates the zeros at $-3.77 \pm 62.7j$ and the poles at $-2.21 \pm 50.7j$. The poles at $-3.77 \pm 62.7j$ then follow trajectories similar to those that the poles at $-2.21 \pm 50.7j$ used to follow in the system shown in Figures 10 and 11.

The similarities between Figures 10 and 12 and between Figures 11 and 13 lead to the conclusion that the 90° difference between expected and actual phase lag of the hydraulic actuator near the second natural frequency of the base does not have a significant impact on the stability of the system.

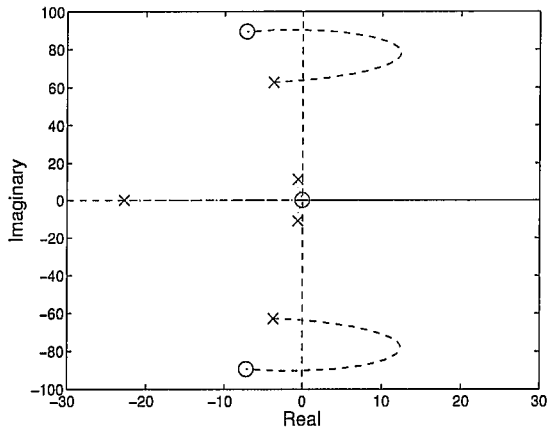

Figure 12. Root locus of the mass damping system with an actuator that is a pure integrator and a first order lag (i.e. the second order pole and zero in the actuator transfer function have some how been removed).

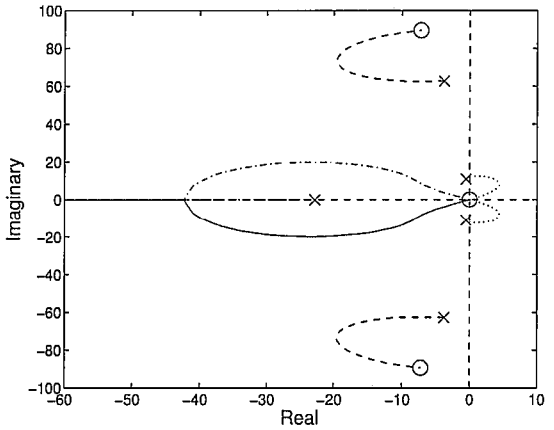

Figure 13. Root locus of the mass damping system with an actuator that is a pure integrator and a first order lag (i.e. the second order pole and zero in the actuator transfer function have some how been removed). The gain K_a is negative.

Consider the second proposed modification: Figures 14 and 15 show the effects on the root locus of switching from accelerometers to sensors that could somehow sense the position of the base. If suitable sensors could be found, this would eliminate another difference between the actual system and the model that this system was designed around. While this difference seems significant, the effects of installing base position sensors on the root locus are not obviously beneficial. This change eliminates a pair of zeros at the origin and changes the system from relative degree zero to relative degree two. Figure 14 shows the root locus with gain K_a positive and Figure 15 shows the root locus with K_a negative. In

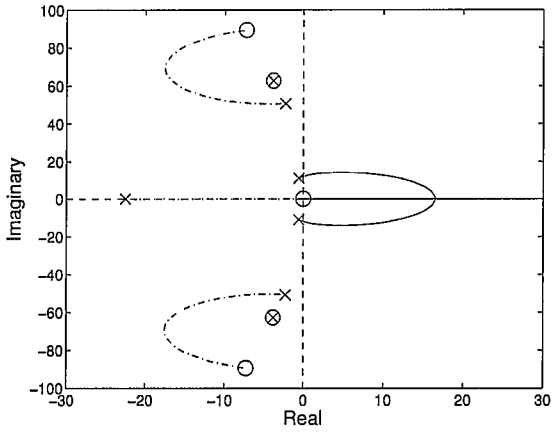

Figure 14. Root locus of the mass damping system with a base position sensor.

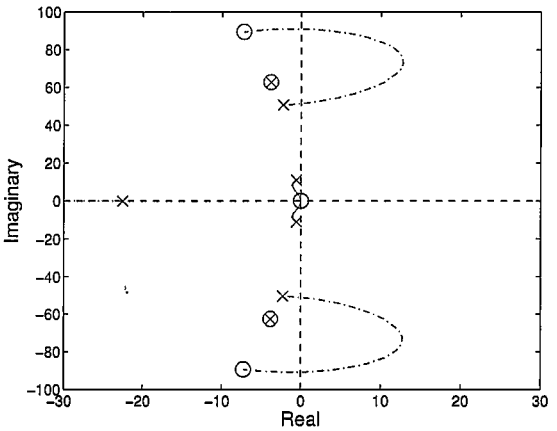

Figure 15. Root locus of the mass damping system with a base position sensor. The gain K_a is negative.

both cases, the system goes unstable before there is a significant improvement in the vibration response.

Root loci were also generated for a system with both of the previously mentioned deviations from the ideal corrected (the actuator is a pure integrator and the system has base position sensors). The system still goes unstable before there is a significant improvement in the vibration response of the system.

Low-pass Filter Design

Figure 16 shows a block diagram of the system with a low-pass filter on the accelerometer feedback signal. Figure 17 shows the root locus of the system with the a low-pass filter cutoff frequency of 2Hz (the filter is a 2^{nd} order Butterworth). This is the first root locus where the poles from both the first and second modes of the flexible base are initially moving

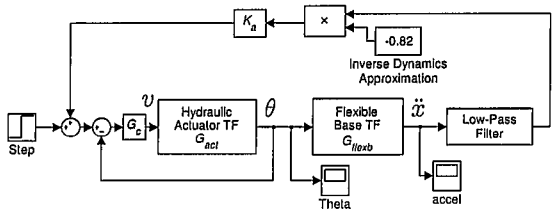

Figure 16. Block diagram of the mass damping control system with a low-pass filter on the accelerometer feed back signal

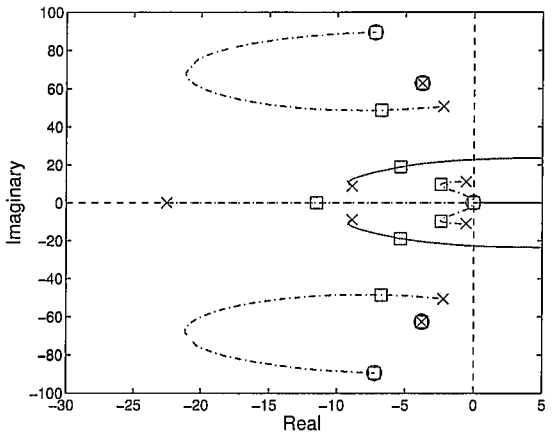

Figure 17. Root locus of the base system with a low-pass filter with a corner frequency of 2Hz.

to the left with increasing gain. This means that damping is being added to both modes for this system.

The squares in Figure 17 show the closed loop pole locations for the gain value of $K_a = 1.75$. The dominant poles are located at $-2.38 \pm 9.79j$, which corresponds to a frequency of 1.6Hz and a damping ratio of $\zeta = 0.24$.

One might consider a higher cutoff frequency to preserve mode one information. Table 1 summarizes the results of root locus analysis for various values of the cutoff frequency f_c. The closed loop response with the maximum damping ratio was found for f_c = 2Hz and $K_a = 1.75$. This agrees with results from experimentally varying the cutoff frequency and gain.

5. Modal State Feedback

As a way to improve the vibration suppression capabilities of the system, it was proposed to add an additional accelerometer and sense the amplitudes of the first two modes. A state feedback controller would then be designed.

Table 1. Summary of the low-pass filter design using root locus. Note that for f_c= 1Hz, $K_a = 8$ is the maximum gain for stability but $K_a = 4.15$ gives the maximum damping for the dominant poles.

		Dominant Pole Location	
Filter Cutoff Frequency (Hz)	Gain (K_a)	Natural Frequency (HZ)	Damping Ratio
1	4.15	2.1	0.084
2	1.75	1.6	0.24
3	1.6	1.6	0.16
4	0.92	1.6	0.12

The modal amplitudes can be found from the accelerometer signals:

$$\begin{bmatrix} \ddot{q}_1 \\ \ddot{q}_2 \end{bmatrix} = \begin{bmatrix} \phi_1(L_1) & \phi_2(L_1) \\ \phi_1(L_2) & \phi_2(L_2) \end{bmatrix}^{-1} \begin{bmatrix} \ddot{x}_1 \\ \ddot{x}_2 \end{bmatrix}. \tag{16}$$

It is desired to place the poles of the two natural frequencies of the flexible base so that $\zeta = 0.7$. To facilitate this, a state space representation of the system will be found starting with the transfer functions

$$\frac{\theta}{v} = \frac{{\omega_d}^2 \left(s^2 + 2\zeta_2\omega_2 s + {\omega_2}^2\right)\tau}{s{\omega_2}^2 \left(s^2 + 2\zeta_d\omega_d s + {\omega_d}^2\right)(s+\tau)} \tag{17}$$

$$\frac{\ddot{q}_1}{\theta} = \frac{s^4 B_1 {\omega_1}^2}{s^2 + 2\zeta_1\omega_1 s + {\omega_1}^2} \tag{18}$$

$$\frac{\ddot{q}_2}{\theta} = \frac{s^4 B_2 {\omega_2}^2}{s^2 + 2\zeta_2\omega_2 s + {\omega_2}^2}. \tag{19}$$

Multiplying equations 18 and 19 by equation 17 allows the transfer functions between input v and outputs $\ddot{q}_1$ and $\ddot{q}_2$ to be found. Placing all three of these transfer functions over a common denominator

$$D = s{\omega_2}^2 \left(s^2 + 2\zeta_d\omega_d s + {\omega_d}^2\right) \cdot (s+\tau)\left(s^2 + 2\zeta_1\omega_1 s + {\omega_1}^2\right) \tag{20}$$

would allow a controllable canonical representation of the system to be found by following the approach in [7, pp.372-374].

Table 2 compares the closed loop pole locations of the current SISO controller to the desired pole locations for the modal state feedback controller. These desired pole locations lead

Current Controller	Modal State Feedback Controller
-177.7	-172.9
$-3.77 \pm 62.7j$	canceled
$-6.75 \pm 48.7j$	$-36.1 \pm 36.8j$
$-5.34 \pm 18.9j$	from filter
$-2.39 \pm 9.74j$	$7.70 \pm 7.85j$
-11.5	-21.8

Table 2. Comparison of closed loop pole locations for the current controller and a modal state feedback controller.

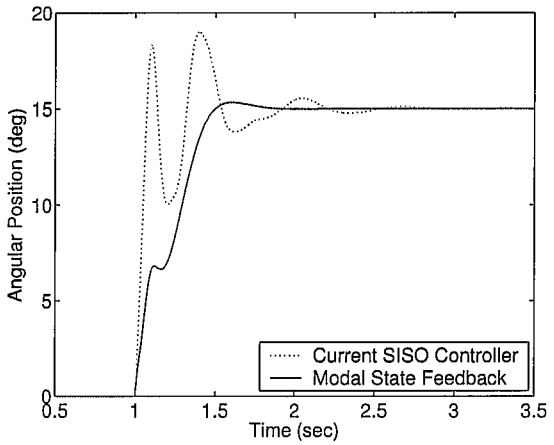

Figure 18. Comparison of the angular position response resulting for two different mass damping controllers.

to the following state feedback gains:

$$K = \begin{bmatrix} 1.21e+09 \\ 1.89e+08 \\ 2.35e+07 \\ 6.06e+05 \\ 1.96e+04 \\ 81.3 \end{bmatrix}. \quad (21)$$

Figures 18 and 19 compare the performance of the current controller to the proposed controller based on modal state feedback. The input to the system is a 15° step change in desired angle. Figure 18 shows the response of angular position θ and Figure 19 shows the base acceleration response. Figures 18 and 19 show that if this controller can be implemented it will improve the response of the system.

6. Conclusions

The primary source of instability in a mass damping controller for a flexible robot was determined. The instability

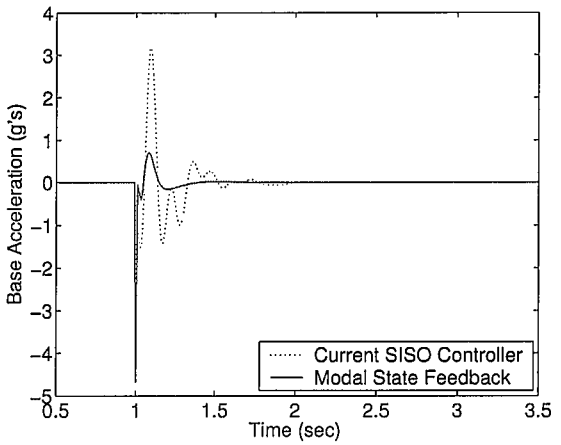

Figure 19. Comparison of the base acceleration responses for two different controllers.

results from the feedback accelerometer moving in opposite directions for the first and second modes of the flexible base for the same input force and torque. This problem was overcome by low-pass filtering the accelerometer feedback signal. The effects of varying the cutoff frequency of the low-pass filter were analyzed using root loci.

A method for improving system performance by state feedback and sensing the amplitudes of the first two modes of the flexible base showed promising results in simulation.

7. Acknowledgments

This research was supported in part by the Fluid Power and Motion Control Center and the HUSCO/Rameriez Chair.

References

[1] Magee, D. P., Cannon, D. W., and Book, W. J., "Combined Command Shaping and Inertial Damping for Flexure Control," *Proceedings of the American Control Conference*, Albuquerque, New Mexico, 1997, pp. 1330–1334.

[2] Loper, J. C., *VIbration Cancellation and Disturbance Rejection in Serially Linked Micro/Macro Manipulators*, Master's thesis, Georgia Institute of Technology, School of Mechanical Engineering, March 1998.

[3] Magee, D. P., Cannon, D. W., and Book, W. J., "Inverse Dynamics for Commanding Micromanipulator Inertial Forces to Damp Macromanipulator Vibration," *IEEE/RSJ International Conference on Intelligent Robotics and Systems*, Albuquerque, New Mexico, 1997, pp. 1330–1334.

[4] George, L. E., *Active Vibration Control of a Flexible Base Manipulator*, Ph.D. thesis, Georgia Institute of Technol-

ogy, School of Mechanical Engineering, Aug. 2002.

[5] George, L. and Book, W. J., "Inertial Vibration Damping Control of a Flexible Base Manipulator," *IEEE/ASME Tansactions on Mechatronics*, Vol. 8, No. 2, 2003, pp. 268–271.

[6] Ogata, K., *Modern Control Engineering*, Prentice Hall, Upper Saddle River, NJ, 4th ed., 2002.

[7] Bay, J., *Fundamentals of Linear State Space Systems*, McGraw-Hill, Boston, 1999.

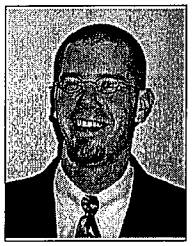

Ryan Krauss *is a Graduate Research Assistant at the Georgia Institute of Technology, Atlanta, GA. His research interests include active vibration suppression and fluid power. Ryan received a B.S. degree in mechanical engineering from Michigan Tech in 1996 and an M.S. degree in engineering mechanics from Virginia Tech in 1998. He is a student member of ASME and IEEE.*

Wayne Book *is the HUSCO/Ramirez Distinguished Professor of Fluid Power and Motion Control at the Georgia Institute of Technology, Atlanta, GA. His research interests include robotics, flexible motion systems, haptics and fluid power and he has authored numerous papers in these areas. Dr. Book received his B.S. from U. Texas at Austin in 1969 and Ph.D. from M.I.T. in 1974, both in mechanical engineering. He is a Fellow in the ASME and IEEE.*